

5107
GE-AK82

Reporting Period: 1 Apr 1981 - 31 May 1982
Contract No. 01-5-022-231
Research Unit No. RU105
Number of Pages 27

ANNUAL REPORT

DELINEATION OF PERMAFROST BENEATH THE ARCTIC SEAS:
SEISMIC OBSERVATIONS IN THE BEAUFORT SEA

Principal Investigators

P.V. Sellmann
K.G. Neave

31 May 1982

Prepared for the BLM-NOAA Arctic Outer
Continental Shelf Environmental Assessment Program

UNITED STATES ARMY CORPS OF ENGINEERS
COLD REGIONS RESEARCH AND ENGINEERING LABORATORY
HANOVER, NEW HAMPSHIRE, U.S.A.

I. Summary

Previous OCSEAP seismic investigations in Harrison Bay (Neave and Sellmann, 1982) provided information on velocity distribution and structure as well as anomalies in the seismic data. This information was used to develop an understanding of permafrost properties and distribution in a major part of Harrison Bay. High-velocity material interpreted to be ice-bonded permafrost was traced as far as 25 km from shore. Permafrost distribution was most variable in the western section of the bay. In the east the depth to the bonded material increases and velocity decreases in an orderly manner with distance from shore. Attenuation zones interpreted to be areas in which the seabed materials contain free gas were also mapped. These attenuation zones and zones of apparent natural seismicity were restricted to the bay and were correlated with high-velocity regions.

Results from this year's program were based on examination of seismic records for the area east of Harrison Bay, including both near-shore ice survey and deeper water marine records. Emphasis was placed on extending interpretations further offshore than those made early in this study (Sellmann and Neave, 1980). Records from as far east as the Canadian border were examined; the main study area is shown on the index map (Fig. 1). The velocity profiles and structure data indicate that ice-bonded permafrost is common in this area, with some regional similarities in the deep velocity data. The results of analysis of near shore data were discussed in Sellmann and Neave (1980). The new records examined extend beyond the offshore islands and add an important perspective to the distribution of high-velocity permafrost. This report is based on a collection of selected seismic lines that link the near-shore data with marine lines that commonly extend as much as 60 km seaward of the small offshore islands. New refraction observations help to document the seaward extent of shallow high-velocity material. The limits of an extremely large, almost anomalously shallow lobe of high-velocity material identified as ice-bonded permafrost were defined. This material extends many kilometers offshore of the Sagavanirktok Delta, often beyond the offshore islands. No equally extensive shallow, high-velocity zones have been observed in other parts of the Beaufort Sea.

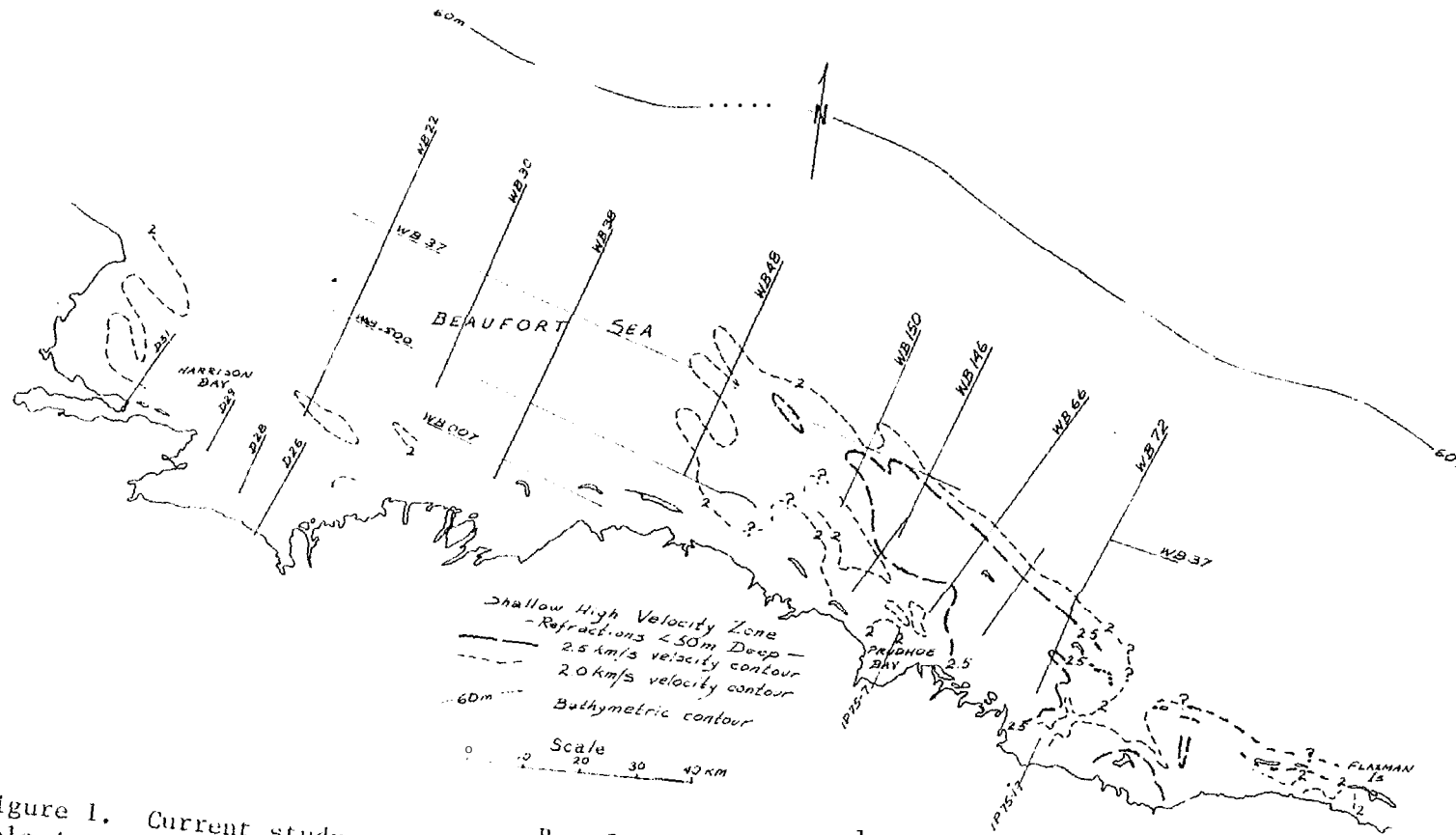


Figure 1. Current study area in the Beaufort Sea showing location of study lines. velocity data indicate distribution of shallow high-velocity layer.

Contoured

Deep reflections recur at approximately 200, 500, and 800 m Throughout this region and the area to the west near Harrison Bay. These reflections commonly extend seaward of the shallower high-velocity material. A histogram of deep reflection data is shown in Figure 2, for the region examined as part of this study. Their depth and configuration appear to correspond with the expected depth to the top and bottom of relict ice-bonded permafrost. The reflections also show patterns that suggest permafrost, with the depth to the top increasing with distance from shore while the depth to the bottom remains fairly uniform.

The noticeable variations in velocity distribution observed along the coast indicate differences in factors such as coastal processes, material types, and geological and thermal history of the region.

II. Introduction

The objective of this annual report is to present the current results and observations made by this work unit since the last annual report (1981) and the recent synthesis report for lease area number 71. It is based on analysis of Beaufort Sea data selected to answer some specific questions regarding the distribution of ice-bonded permafrost. Lines were picked to obtain more information on the offshore extent of the deep relict ice-bonded permafrost, and the distribution of shallow, high-velocity, ice-bonded permafrost. The study area and lines examined are shown in Figure 1.

The Harrison Bay investigation discussed in our 1981 annual report was also completed and formalized as a CRREL Report (in press).

The information on offshore permafrost distribution and properties was inferred from consideration of velocities and structures from both refraction and reflection analysis. The resulting velocity data were used to construct velocity profiles and velocity distribution maps.

111 Current State of Knowledge

Most available information on subsea permafrost has been acquired as part of government-supported studies. Much of this information is based on OCSEAP investigations. As a result of these studies we are gaining an understanding of the variable nature and great extent of ice-bonded subsea permafrost in the Beaufort Sea, as well as patterns of permafrost distribu-

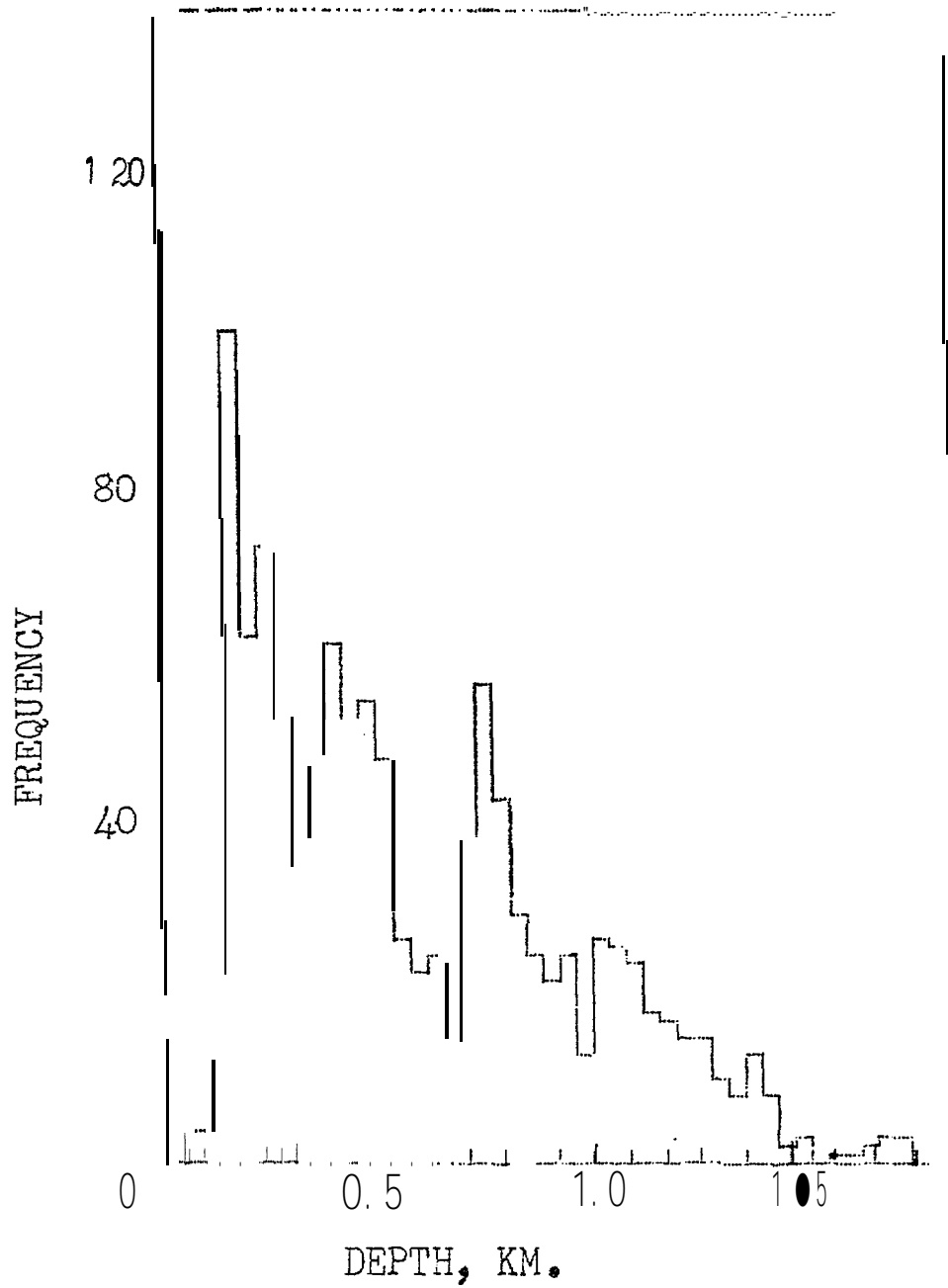


Figure 2. Histogram of depths of subsea reflections for the Harrison Bay and Beechey Point quadrangles. Note the three distinct peaks at 200, 450, and 750 meters.

tion in this region. The small amount of information from the Chukchi Sea suggests that distribution of ice-bonded permafrost will be much more restricted than in the Beaufort Sea. Seismic studies are the basis for much of our distribution data. Unfortunately, there is little or no supporting drilling data for use in control and calibration of the seismic data. Requirements still exist for information on permafrost thickness, offshore extent, ground ice distribution, and zones where shallow ice-bonded materials occur. This information is needed for the development of predictive permafrost models, for understanding unique subsea permafrost processes, and for establishing regional permafrost distribution patterns.

This study was directed at obtaining more information on the above topics. Fortunately the observations were also made where the greatest amount of control exists based on earlier drilling and sampling efforts that were part of the USGS Conservation Division and OCSEAP studies.

Additional topics for which more data are needed that require drilling efforts include: engineering properties of frozen saline sediments, distribution data from drilling for control purposes and for establishing distribution patterns, and distribution of permafrost and frozen sediment related features such as overconsolidated materials and gas in both free and hydrate form.

IV. Study Area

The general location of the area covered in this report and the lines from which data were selected for analysis are shown in Figure 1.

V. Sources, Methods and Rationale of Data Collection

The basis for this study is that noticeable changes in seismic velocities occur between frozen and unfrozen unconsolidated materials. This fact and the existence of large amounts of seismic data from surveys conducted for petroleum exploration make studies-of the distribution of ice-bonded subsea permafrost by seismic techniques a reasonable approach. When records are available, and their quality and field-recording parameters are appropriate, permafrost data can be extracted.

Three types of waves have been identified on the monitor records and used in the analysis: refractions, reflections, and surface waves. The same analysis procedure is used for all three wave types. Each reading of a

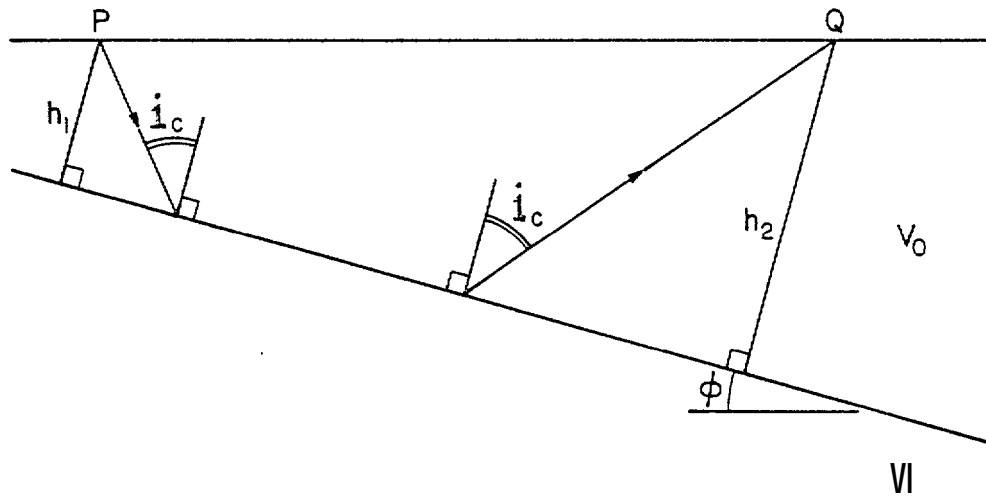


Figure 3. Ray path geometry for a refractor dipping at an angle ϕ . The shot is at P and the receiver is at Q for the down-dip shot. The shot and receiver positions are reversed for the up-dip shot.

record consists of the coordinates (x and t) for the tangent point on the time-distance plot plus a slope measurement ($c = dx/dt$) of a tangent to the curve. This information is converted to velocity data and depth profiles by means of the appropriate equations described below.

Refractions

A dipping plane layer refraction interpretation could be used on the reversed ice shooting records. Following the derivation given by Grant and West (1965) and using the geometry shown in Figure 3, the critical angle is given by $i_c = \sin^{-1}(V_0/V_1)$, where V_0 is the upper layer velocity and V_1 is the lower layer velocity. The apparent velocity in the lower layer when shooting down-dip is

$$c^- = V_0/\sin(i_c + \phi) = V_0/\sin[\sin^{-1}(V_0/V_1) + \phi] \quad (1)$$

where ϕ is the dip of the boundary. For shooting up-dip, the apparent velocity is

$$c^+ = V_0/\sin(i_c - \phi) = V_0/\sin[\sin^{-1}(V_0/V_1) - \phi] \quad (2)$$

Equations 1 and 2 can be combined to give an expression for the true velocity (V_1) in the lower layer.

$$\begin{aligned} 1/c^- + 1/c^+ &= \sin(i_c + \phi)/V_0 + \sin(i_c - \phi)/V_0 \\ &= 2 \sin i_c \cos \phi / V_0 \\ &= 2 \cos \phi / V_1. \end{aligned}$$

For small dip angles,

$$1/V_1 = 1/2 (1/c^- + 1/c^+). \quad (3)$$

Grant and West show that the distance h from the up-dip shot point to the high-velocity refractor is

$$h_1 = (V_0 t_0^-/2) [1 - (V_0/V_1)^2]^{-1/2} \quad (4)$$

where t_0 is the intercept time on the record. We did not measure the intercept time, but it can be easily calculated from the tangent readings. This converts eq 4 to

$$h_1 = (V_0/2) (t^- - x-/c-) [1 - (V_0/V_1)^2]^{1/2}. \quad (5)$$

For purposes of constructing seismic cross sections, the depths were plotted under the midpoints of the reversed spread. An average depth (h) was calculated for an array based on values from its ends:

$$\bar{h} = (V_0/4) (t^- + t^+ - x-/c- - x^+/c^+) [1 - (V_0/V_1)^2]^{1/2}. \quad (6)$$

Equations 3 and 6 are the required equations for making velocity and depth profiles for the ice shooting data.

There are no reversed profiles for the marine survey data; therefore, they were interpreted assuming plane horizontal layers. Equations 2 and 5 can be rewritten for horizontal layers by setting $\phi = 0$ and $c^- = c^+$:

$$V_1 = c \quad (7)$$

$$h = (V_0/2) (t - x/c) [1 - (V_0/V_1)^2]^{1/2}. \quad (8)$$

These two equations allow the conversion of tangent readings from the marine records to velocity and depth profiles along the marine lines.

Reflections

Reflection data analysis was based on assuming a plane horizontal reflector at a depth h under a uniform upper layer with velocity V_0 . This simple model results in the equation of a hyperbola for the travel time t and the distance x from the shot point to the receiver (see Grant and West, 1965):

$$V_0^2 t^2 = x^2 + 4h^2. \quad (9)$$

Taking differentials on both sides of the above equation gives an expression for the upper layer velocity:

$$2V_0^2 t dt = 2x dx. \quad (10)$$

Since $dx/dt = c$, eq 10 can be arranged to give the velocity in terms of the tangent readings:

$$v^* = (cx/t)^{1/2}. \quad (11)$$

Combining eq 9 and 11 gives an expression for the depth to the reflector:

$$h = (x/2) (et/x - 1)^{1/2}. \quad (12)$$

Any tangent to a reflection curve can be converted using eq 11 and 12 into a depth and velocity determination for profile construction along the shot lines. Where possible, a number of tangents were read on each reflector, so that scatter on the plotted reflecting horizons could help to indicate the accuracy of the determinations.

Rayleigh Waves

Based on the surface wave or Rayleigh wave tangent measurements, profiles were made of the phase velocity along the survey lines.

Spatial Resolution

The spatial resolution of the data from this type of study is obviously not as great as can be obtained from a seismic investigation specifically designed to study offshore permafrost. For refraction and reflection measurements, a number of factors must be considered, including geophone spacing, signal frequency, and complexity of the subsurface. In general, the horizontal extent of a feature that can be detected should be a minimum of three detector spacings. This means that the **minimum size** of a target that can be resolved is around 300 m for the ice-shooting data, and around 150 m for the marine survey data. The minimum vertical thickness of a detectable high-velocity layer is determined by the wavelength of the refracted signal (Sherwood, 1967). Resolution is possible to approximately 1/2 wavelength or about 50 m for these data. In addition, Sherwood's results show that thin layers (less than 30 m thick) might be observed at shallow depths, but the signals from these would be in the form of plate waves at a reduced velocity and amplitude.

A simplifying assumption was used for the refraction depth determinations. The upper layer velocity was taken as 1.8 km/s for all profiles. This means that the water layer, 0 to 16 m deep, was combined with the low-velocity bottom sediments to make a single upper layer. Upper-layer velocities were observed to range from 1.6 to 2.0 km/s. Therefore, the

error introduced by assuming 1.8 km/s could be as much as 30% under rare circumstances (see Error Estimates).

Refraction velocities and depth determinations from single-ended marine records are subject to errors caused by dipping layers. Our interpretations indicate that dips are normally less than 3%. The corresponding maximum error is approximately 5% in velocity measurements and 2% in depth determinations, as discussed in the following section.

The assumption of horizontal layers for the reflection interpretation does not result in significant errors. The following error calculations show that a 3% dip usually results in a 1% error in velocity and 2% in depth.

Error Estimates

The first error estimate arises from using an average upper layer velocity of 1.8 km/s for refraction calculations instead of the local value. A worst case situation is examined to illustrate how much error is introduced. The remaining error problems involve dipping layers when the interpretation assumes horizontal layers. For these cases, we used typical readings and calculated the difference between the velocity and depth estimates for horizontal layers and layers with a 3% dip.

When the correct local velocity V_L is used in eq 8 of the Methods section, the depth is:

$$h_L = (t - x/c) (V_L/2) [1 - (V_L/V_1)^2]^{-1/2}. \quad (13)$$

When the average velocity $V_A = 1.8$ km/s is used instead, the erroneous depth estimate is

$$h_A = (t - x/c) (V_A/2) [1 - (V_A/V_1)^2]^{-1/2}. \quad (14)$$

The proportional error in the depth estimate is

$$\begin{aligned} (h_L - h_A)/h_L &= 1 - h_A/h_L \\ &= 1 - \frac{V_A}{V_L} \left[\frac{1 - (V_L/V_1)^2}{1 - (V_A/V_1)^2} \right]^{1/2} \quad (15) \end{aligned}$$

This expression gives the largest error when the local velocity is large and the lower layer velocity V_1 is small. We can choose $V_L = 2.0$ km/s and $V_1 = 2.3$ km/s (Neave and Sellmann, in press). This highly unlikely combination of velocities results in an error of 30%.

The effects of dip on the interpretation of apparent lower layer velocity from single-ended refraction data can be found from eq 1:

$$c = V_0 / \sin [\sin^{-1} (V_0/V_1) + \phi]. \quad (16)$$

The real velocity in the lower layer can be found by solving this equation for V_1 :

$$V_1 = V_0 / \sin [\sin^{-1} (V_0/c) - \phi]. \quad (17)$$

The proportional error in the lower velocity from using a horizontal layer model is

$$\begin{aligned} (v_1 - c)/V_1 &= 1 - c/V_1 \\ &= 1 - (c/V_0) \sin [\sin^{-1} (V_0/c) - \phi]. \end{aligned} \quad (18)$$

The estimated depth for the horizontal layer model is given by eq 8:

$$h_H = (V_0/2) (t - x/c) \left[1 - (V_0/c)^2 \right]^{-1/2} \quad (19)$$

This equation can have V_1 replaced by a substitution from eq 17. Then eq 19 and 20 can be used to find the proportional error in the depth:

$$(h_D - h_H)/h_D = 1 - \cos [\sin^{-1} (V_0/c) - \phi] [1 - (V_0/c)^2]^{-1/2}. \quad (20)$$

Using a typical set of velocities, $V_0 = 1.8$ km/s and $c = 3.66$ km/s. A slope of 3% results in a 2% error in depth according to eq 21, and the corresponding error in the velocity is 5% from eq 18.

For the reflections from a plane boundary which dips at an angle ϕ , the arrivals on the record still form a hyperbolic curve; however, the hyperbola is not centered with respect to the shot point. The arrival times can be calculated from an image source R (Fig. 4) which is at a depth $h = 2h \cos \phi$ and displaced by a horizontal distance $\xi = 2h \sin \phi$ from the true source P .

The travel time equation is

$$t^2 = \frac{(X + \xi)^2 + (2h \cos \phi)^2}{V_0^2}$$

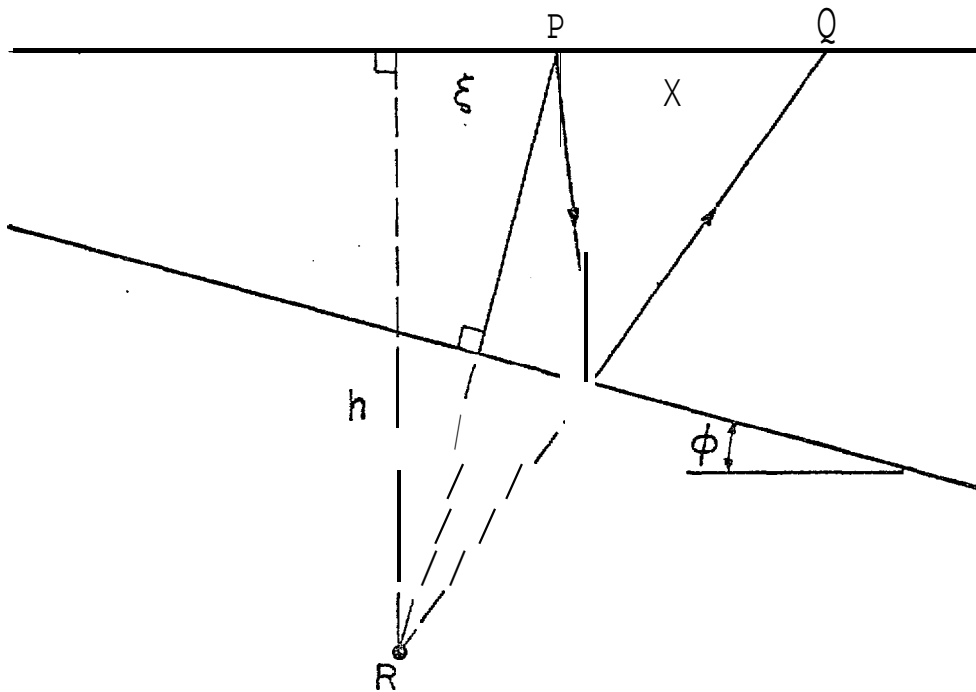


Figure 4. Raypath geometry for a reflector dipping at an angle ϕ .

$$t^2 = (1/V_0^2) (4h^2 \cos^2 \phi + 4h^2 \sin^2 \phi + 4hx \sin \phi)$$

$$t^2 V_0^2 = 4h^2 + x^2 + 4hx \sin \phi. \quad (21)$$

Taking differentials on both sides of the equation gives

$$2t V_0^2 dt = 2x dx + 4h \sin \phi dx$$

$$V_0^2 = (x/t) (dx/dt) + (2h \sin \phi / t) (dx/dt). \quad (22)$$

The estimated velocity for the horizontal layer interpretation was

$$V_H = \left(\frac{x dx}{t dt} \right)^{1/2} = \left(\frac{cx}{t} \right)^{1/2}. \quad (23)$$

This can be substituted into eq 23:

$$V_0^2 = V_H^2 + 2h \sin \phi V_H^2 / x$$

$$V_0 = V_H [1 + 2h \sin \phi / x]^{1/2}. \quad (24)$$

The proportional error in velocity is

$$(V_0 - V_H) / V_0 = 1 - [1 + 2h \sin \phi / x]^{-1/2} \quad (25)$$

Now compare the horizontal layer depth estimate in eq 12

$$h_H = (x/2) [(ct/x) - 1]^{1/2}$$

to the distance to the reflector in eq 22

$$t^2 V^2 = 4h^2 + x^2 + 4hx \sin \phi.$$

To eliminate V_0 , we use eq 24 and 25:

$$ctx [1 + (2h \sin \phi / x)] = 4h^2 + x + 4hx \sin \phi.$$

This is rearranged as a quadratic equation with h as the unknown:

$$4h^2 - (4x \sin \phi - 2ct \sin \phi) h - (x^2 - ct^2) = 0. \quad (26)$$

Solving for h gives

$$h = (1/8) (2ct - 4x) \sin \phi \pm (1/8) [(2ct - 4x)^2 \sin^2 \phi - 16(ct^2 - ct^2 x)]^{1/2}$$

$$= [(et/4) - (x/2) \sin \phi \pm (1/4) (et - 2x)^2 \sin^2 \phi - 4(x^2 - ctx)]^{1/2} \quad (27)$$

The relative error in depth is

$$\frac{\Delta d}{d} = \frac{(x/2) [(et/x) - 1]^{1/2}}{1/4 (et-2x) \sin \phi \pm 1/4 [(et-2x)^2 \sin^2 \phi - 4x(x-et)]^{1/2}} \quad (28)$$

For a typical reflection reading, $c = 2.0$ km/s, $x = 1.0$ km and $t = 0.63$ s. With a dip of 3% on the reflector, we find a 1% error in the velocity determination and a 2% error in the depth.

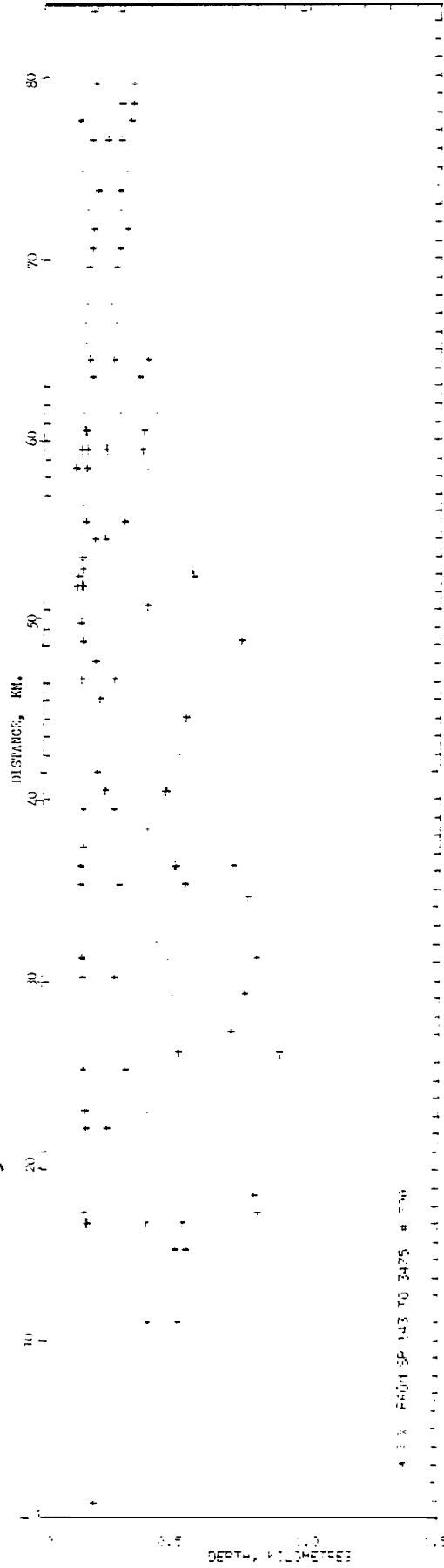
VI and VII Results and Discussion

Reflection Data

Reflection analysis of returns in this region indicates that three deep horizontal reflecting horizons are common (Figure 2). The depths of these reflectors are approximately 200, 500 and 800 meters. These features are not continuous on all lines but can be found repeatedly throughout the region. An example of good continuity in the reflectors can be seen in Figure 5a. This line (W8 500) is an east-west section on which the upper reflector is a continuous feature for the entire length of the line. The intermediate reflector is missing on the eastern t'bird of the line, while the deep reflector is suggested by a scattering of reflections between 700 and 900 m. However, the deep reflector is not continuous enough to define a single horizon. Additional examples of the continuity of the reflectors can be seen in Figures 5b and c, which are the north-south lines WB66 and WB22. The north halves of both lines show reflection horizons at 500- and 800-m depths. In Figure 5c a segment of the 200-m upper reflector can be found at the north end of the line, with the intermediate reflector seen at the south end. The west end of line WB37 is reproduced in Figure 5d with a good example of a strong continuous reflector at 800 m. The 200-m reflector is well represented on this line, as well as a small segment of the 500-m reflector.

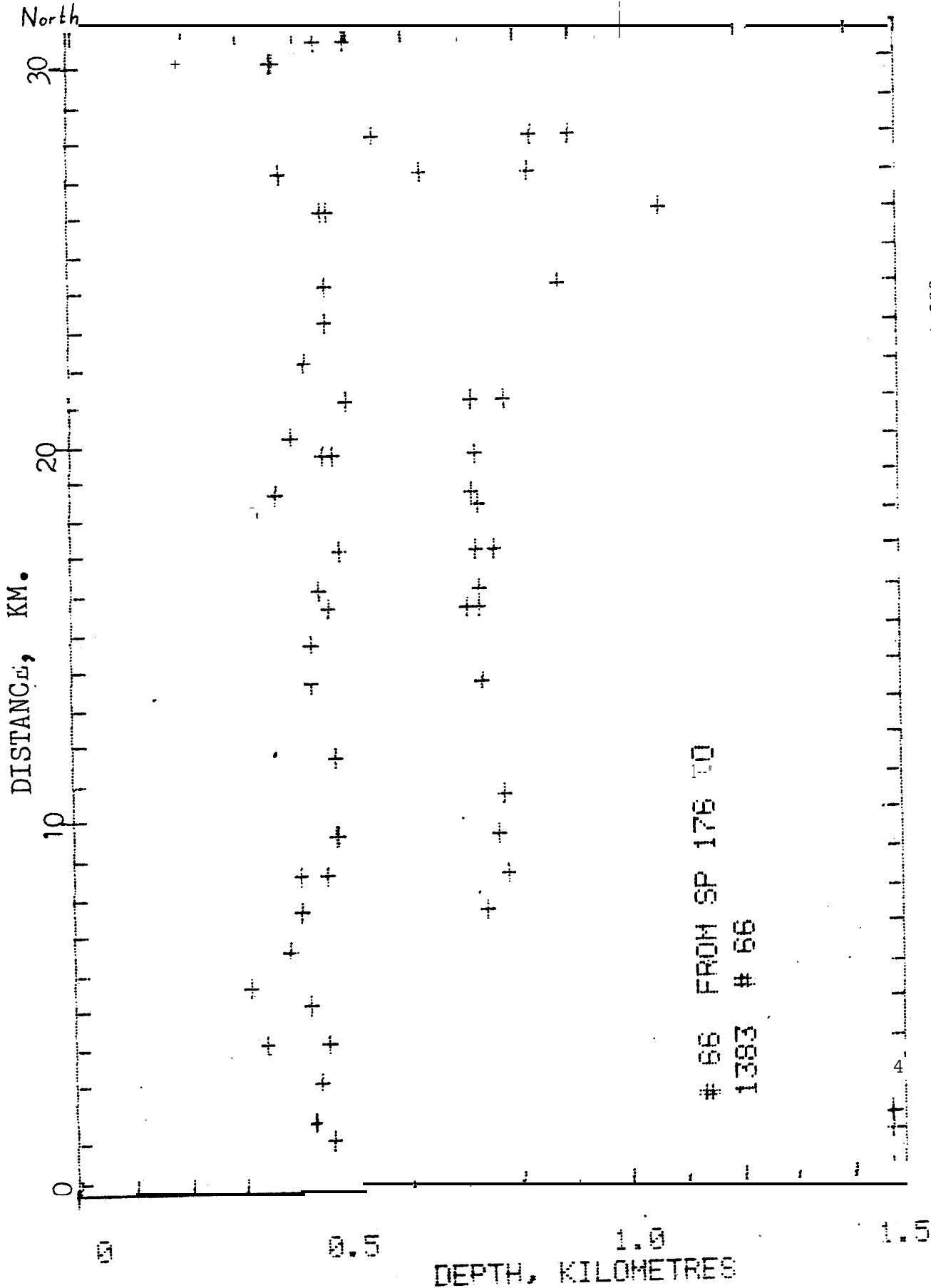
Refraction Data

Probably the most significant results that developed from the new refraction analysis was establishing the wide distribution of shallow high-velocity material in the region offshore of the Sagavanirktok Delta and obtaining information in its limits. Refraction data in Figure 6a, from



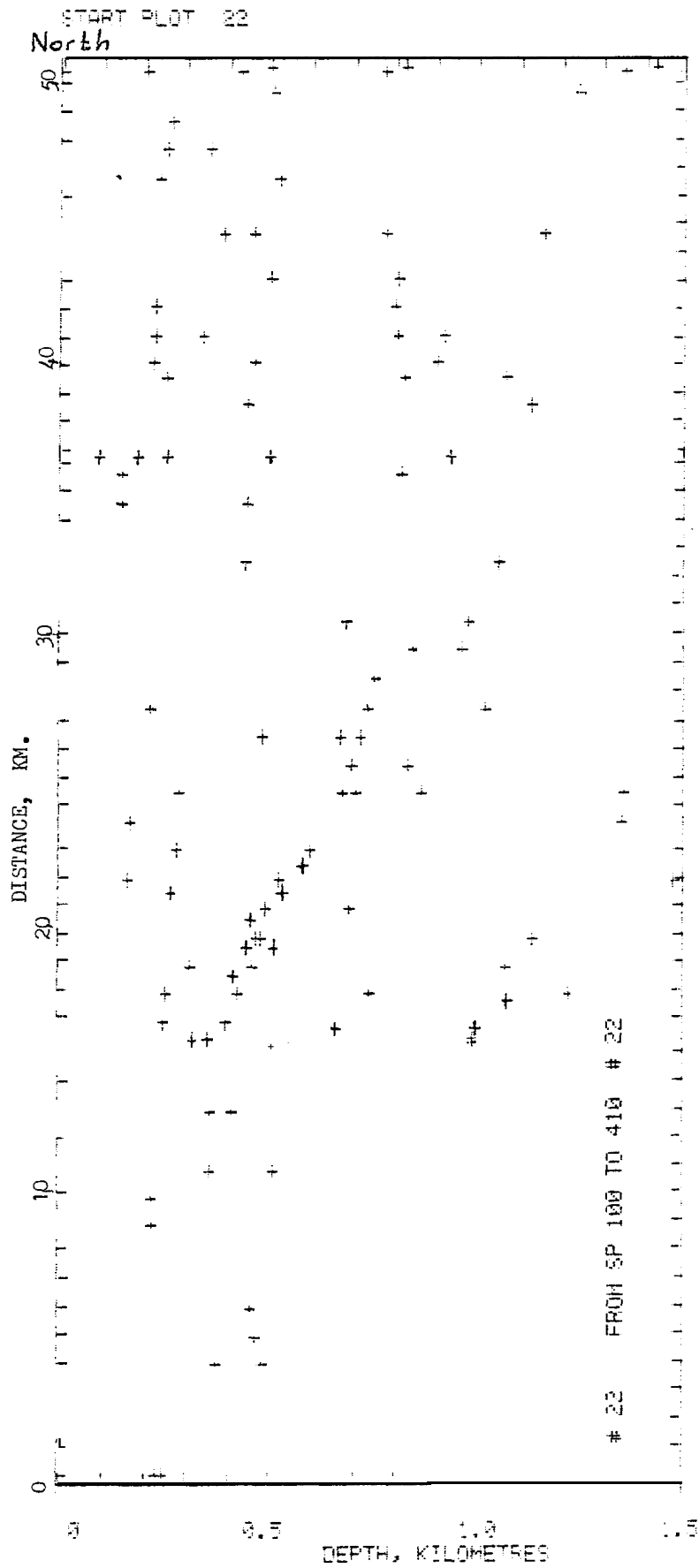
a. Line WB500 with reflections at approximately 200 and 500 m.
 Figure 5. Reflection sections showing horizontal structures.

START PLOT 66



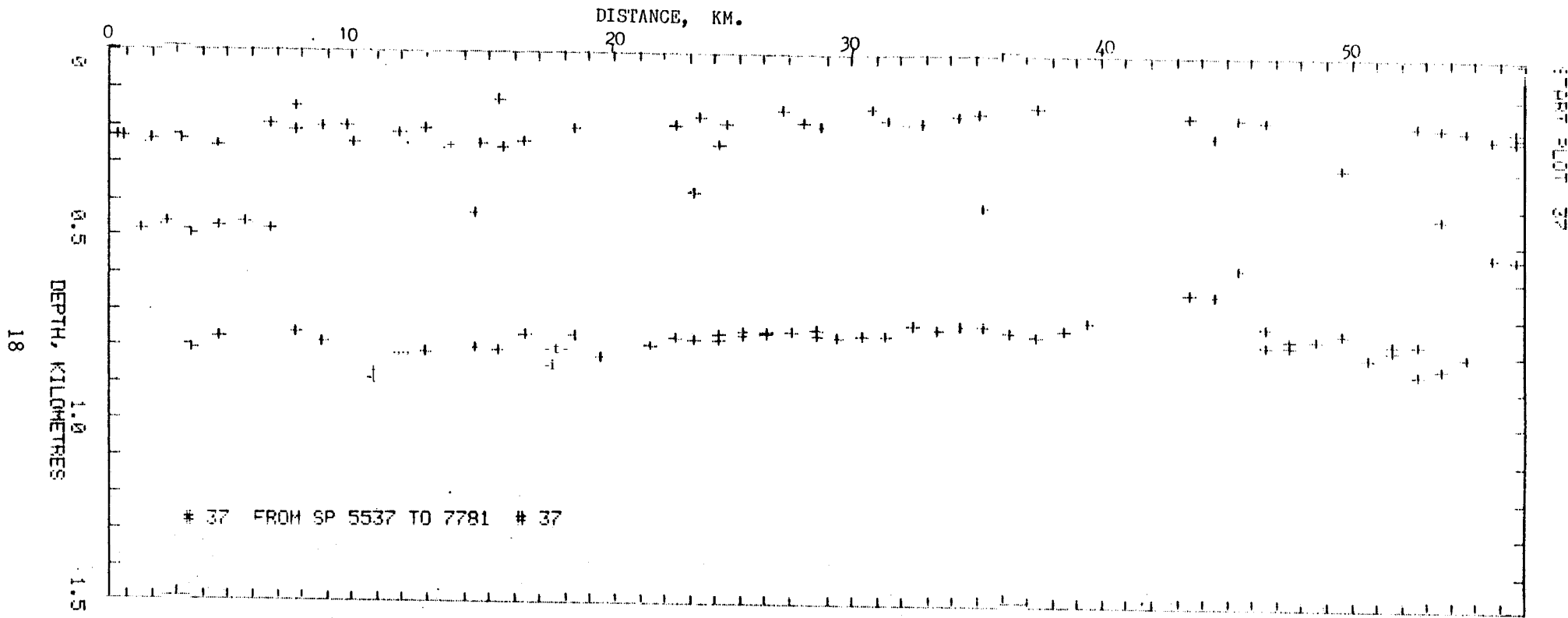
B. Line WB66 with reflectors at approximately 500 and 800 m.

Figure 5 (cont'd). Reflection sections showing horizontal structures.



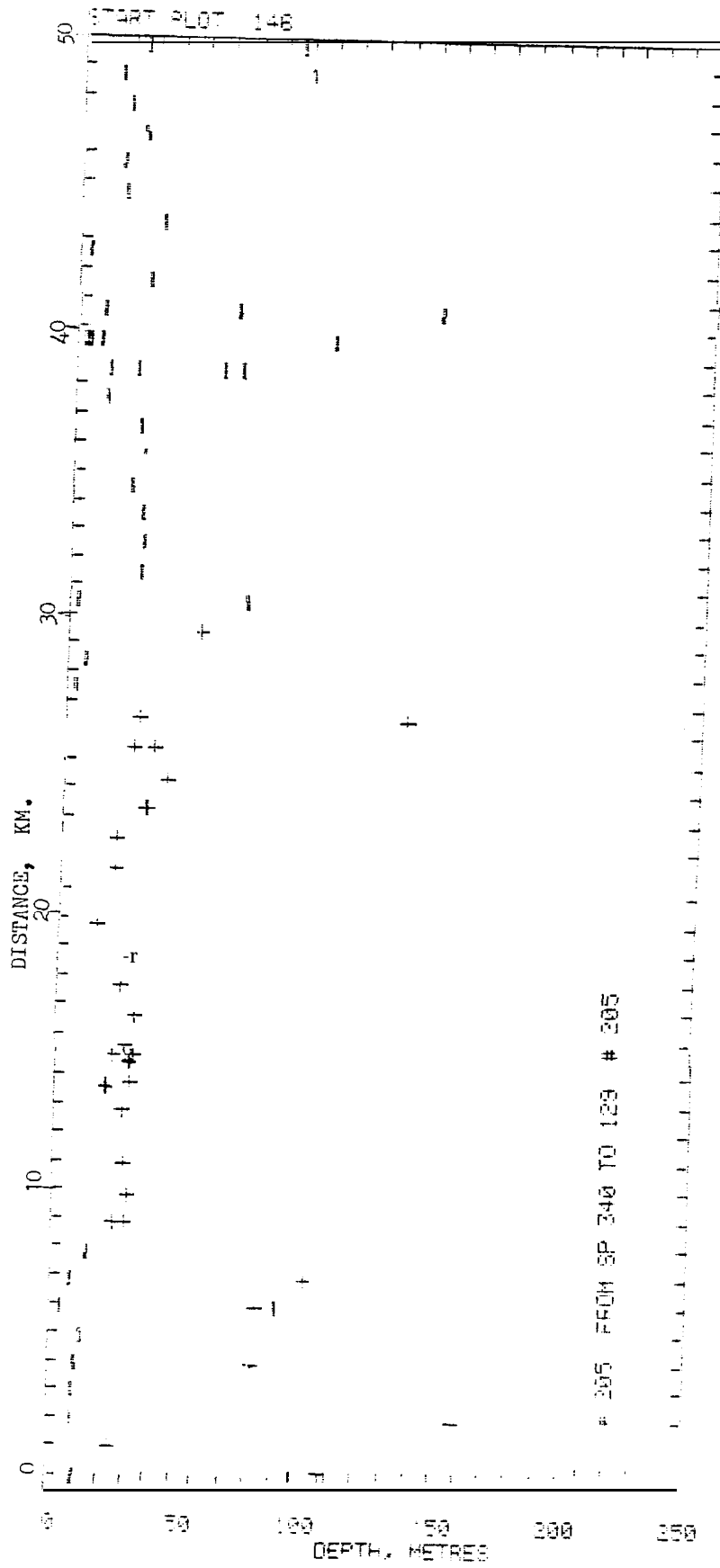
c. Line WB22 with reflectors at approximately 200 and 500 m.

Figure 5 (cont'd).

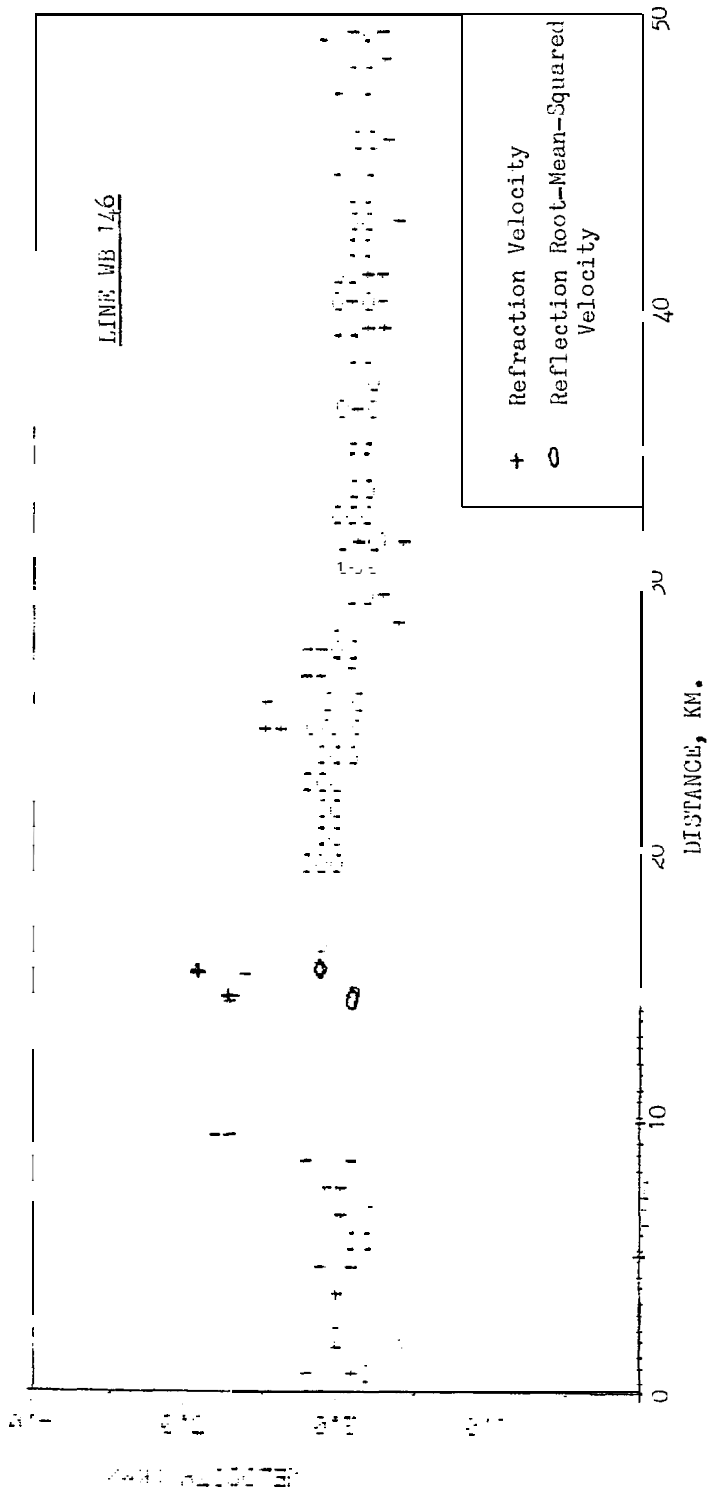


d. The west half of line WB37 with reflectors at approximately 200, 500 and 800 m.

Figure 5 (cent'd). Reflection sections showing horizontal structures.



a. Depth to the refractors. - indicates velocity < 2 km/s, and + indicates velocity > 2 km/s.
 Figure 6. Refraction profiles for line WBI46.



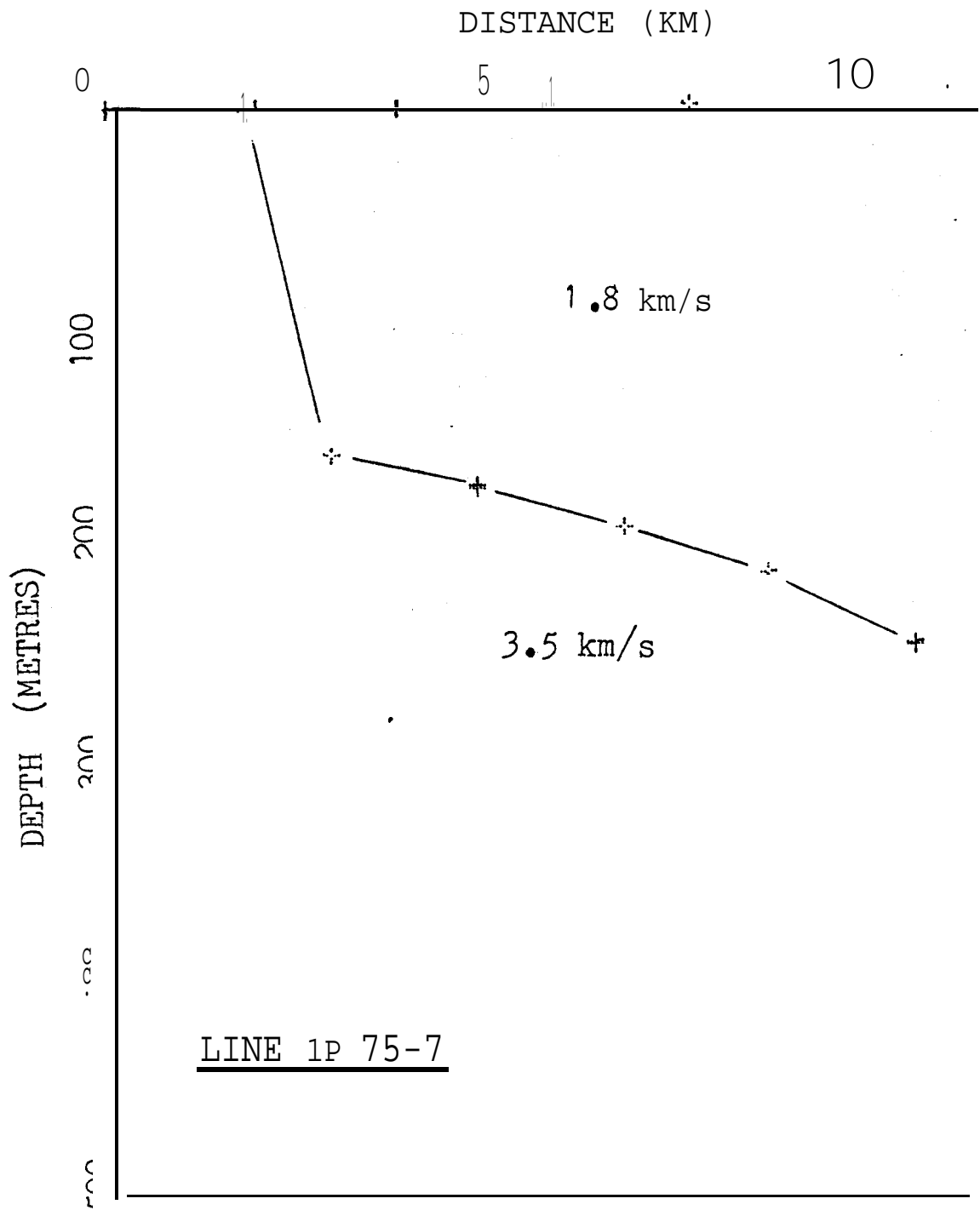
b. Velocity profile.

Figure 6 (cont'd). Refraction profiles for line WB146.

line **WB146** north of Reindeer Island, show the high velocities observed in the sediments very close to the seabed. The top of the high-velocity material is seen at 20 to 40 m below sea level. On this line the **high-velocity** segment (>2 km/s) is confined to a 17-km-long section that starts adjacent to Reindeer Island. A corresponding velocity profile (Figure **6b**) for line **WB146** shows the abrupt beginning of the high velocity material along with a steady decrease in velocity with distance north of the island. The maximum velocity **on** this line is approximately 3 km/s and the minimum is 1.7 km/s for the seabed refractor.

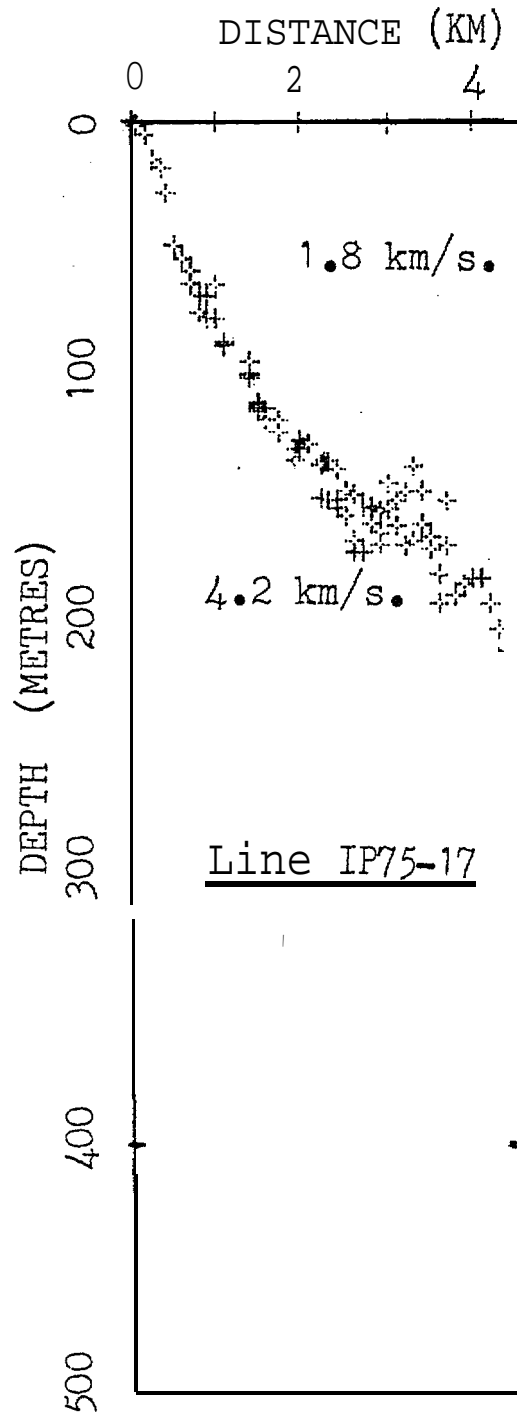
The shallow high-velocity material is found in the extensive region shown in Figure 1 enclosed by the 2-ion/s velocity contour. The northeastern boundary of this region parallels the 20-m **isobath**. Drilling results from the Hardy-Lawson program suggest that this zone extends to the east on the offshore side of the barrier islands. The western boundary of this zone occurs between the Sagavanirktok and **Colville** rivers at approximately $139^{\circ} 30'$ west longitude. The high velocity zone does not exist **immediately** south of Reindeer Island, even though it can be found to the southeast, extending offshore from the **Sagavanirktok** Delta. South of Reindeer Island a **refractor with** a velocity of 2.2 km/s is found at a depth of 130 m. Deep refractors much **like** this are **also** found throughout this region. Examples are shown for **Prudhoe Bay (Fig. 7a)**, **Foggy Island Bay (Fig. 7b)** and **Harrison Bay (Fig. 8)**. These deep refracting layers only approach the surface at the coastline, where they rise to correspond with the shallow high-velocity permafrost on land. The offshore extension of these lines appears to correspond with the 200-m reflector observed on the marine records.

Therefore, there is some evidence that the 200-m reflection is **the** top of the thick **slab** of relict subsea permafrost. An example of the apparent continuity of this structure from the refractions and reflections in the coastal and marine survey data is shown **by** comparing the north ends of lines D26 and 28 and the south **end** of line **WB22**. The approximate 200-m-deep refractor on the north end of the D lines (Figure 8) corresponds to the intermittent 200-m-deep reflector at the south end of the **WB** line (Figure **5c**).



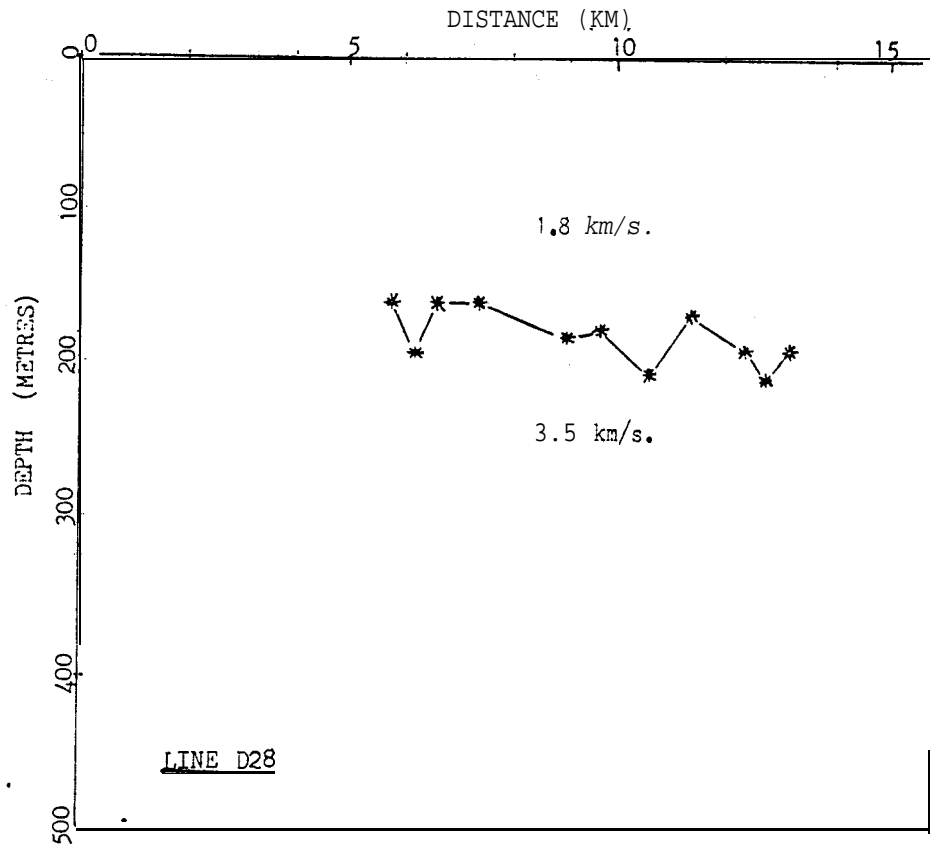
a. Line 1P 75-7 has a relatively flat refractor just above 200 m.

Figure 7. Refraction sections from Prudhoe Bay and Foggy Island Bay.

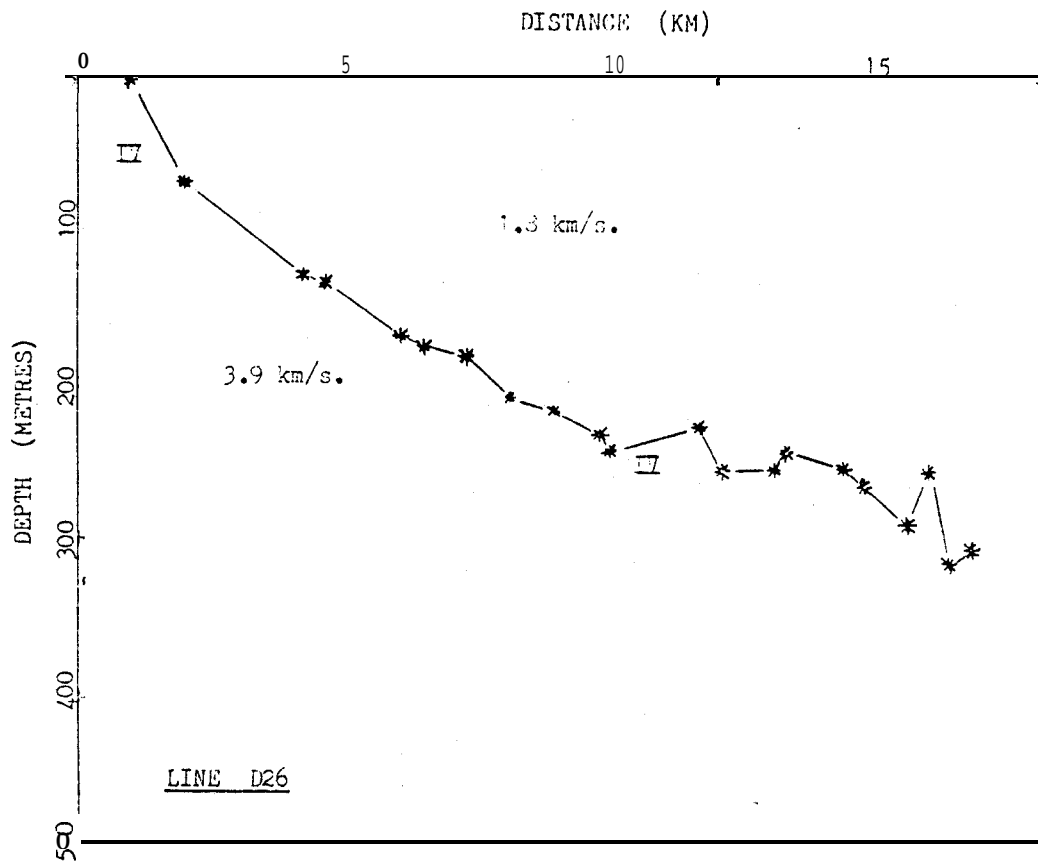


3. Line IP 75-17 has a layer dipping at approximately 2.5%.

Figure 7 (cent'd),



a. Line D28 has a flat refractor just above 200 m.



b. Line D26 has a refractor dipping at 2.2%.

Figure 8. Refraction sections from Harrison Bay.

The intermediate reflector at the approximate depth of 500 m coincides with the depth of permafrost on land in some parts of this area based on analysis of onshore well data (**Osterkamp** and Payne, 1981). This reflector may represent the velocity contrast between the ice-bonded sediments in a relict permafrost layer and the warmer thawed sediments below. Even though the position of this reflector corresponds with the observed depth of on land ice-bonded permafrost along segments of this coastline, the evidence is not as conclusive as for the source of the upper reflector.

Additional evidence that suggests the near horizontal reflectors are permafrost related is that they appear to be cut by dipping structures. The dipping **strucutres** would most likely be related to changes in material type, with the horizontal features related to contrast in the change of state of the pore water. The base of the permafrost should be fairly uniform with distance from shore in an area of active coastal retreat. Increases in the depth to the top of ice-bonded material with distance from shore should be more noticeable.

The source of the 800-m reflector is not known. It **is likely** related **to** some change in material types; however, it has been suggested that it may be related to the distribution of hydrates.

The information on the distribution of the shallow high velocity material shown in Figure 2 helps to illustrate the great local extent of this ice-bonded permafrost unit. Test drilling in this zone helps support the results of the seismic analysis. The holes drilled off the **Sagavanirktok** and beyond the offshore islands to the east indicate that the top of this shallow unit ranged in depth from 7 to 24 m below the seabed (Harding and Lawson Associates, 1979).

VIII Conclusions

Shallow high-velocity zones of ice-bonded permafrost occur locally in the Beaufort Sea. The largest unit observed occurs off the **Sagavanirktok** Delta where ice-bonded sediments are commonly found less than 10 m below the seabed.

A general **pattern** seems to exist for the deeper high-velocity material. Refractors can often be traced from the surface on land to depths in excess of 150 m where they correspond to a reflecting horizon commonly found at 200 m. Because of **the** apparent link with the high velocity permafrost on shore the evidence is strong for this being the top

of ice-bonded permafrost off shore. Variation in the depth to this first high velocity layer depends locally on material type and geological history of the region. The general pattern is for the velocity to decrease **with** distance from shore until the unit is no longer detectable. This decrease in velocity with distance from shore makes determining the limit of **ice-**bonded permafrost difficult. Current analysis suggests that ice-bonded material will occur beyond the limits of the lines **stuides**, out to at least 55 km from shore.

Reflectors at 500 and 800 m are also common. The 500-m reflector may correspond to the base of permafrost.

The deeper permafrost unit can be overlain by the shallow **high-**velocity material in some areas. This shallow unit may form after degradation of the deep unit is initiated. Examples of this are found in areas where perennial freezing of the bed may occur in association with the formation of shoals or islands. Shoreward movement of the barrier islands could also account for the shallow ice-bonded material found seaward of these islands, particularly for those where **only** deep ice-bonded material is observed on the shoreward side. Reindeer Island and **the** chain in the eastern part of the study area may be examples of this situation.

Cases where shallow high-velocity material will not be separated from deep ice-bonded permafrost will be found near shore in zones of active coastal erosion such as in the western part of lease area 71.

The origin of the shallow zone shown in Figure 1 is not known. It may be related to a more recently degraded **land** surface.

Reference List

- Grant, F.S. and G.F. West (1965) Interpretation Theory in Applied Geophysics, New York: McGraw-Hill.
- Harding-Lawson Associates (1979) **Geotechnical** Investigations, Beaufort Sea, Contract Report prepared for the Conservation Division of the USGS. USGS data Set AK-17718, Vol. 1-3.
- Neave, K.G. and P.V. Sellmann (1982, in press) Subsea Permafrost in Harrison Bay, Alaska: An Interpretation from Seismic Data, USACRREL Report.
- Osterkamp, T.E. and M.W. Payne (1981) Estimates of Permafrost Thickness from Well Logs in Northern Alaska, **Journal of Cold Regions Science and Tehnology**, vol. 5, p. 13-27.
- Sellmann, P.V. and K.G. Neave (1980) Delineation and engineering characteristics of permafrost beneath the Beaufort Sea. Environmental Assessment of the Alaskan Continental Shelf, **Annual Report**, vol. IV, p. 125-157.
- Sherwood, J.W.C. (1967) Refraction along an embedded high-speed layer. In: **Seismic Refraction Prospecting** (A.W. Musgrove, Ed.), Society of Exploration Geophysicists, Washington, p. 138-151.